Molecular Accessibility in Relation to Cell Surface Topography and Compression Against a Flat Substrate

Sandrine A. Hocdé,[†] Ollivier Hyrien,[‡] and Richard E. Waugh[†*]
[†]Department of Biomedical Engineering and [‡]Department of Biostatistics and Computational Biology, University of Rochester, Rochester, New York

ABSTRACT The recruitment of cells to the vascular wall in vivo or the capture of cell subpopulations at the surface of a fabricated device requires the formation of bonds between specific molecular pairs on the cell and the substrate. The ability of a molecule to form a bond depends critically on its localization relative to the cell surface topography. In this report, we present a framework for the quantitative assessment of molecular availability that accounts for the deformability of the cell surface and the balance of forces in the interface, as well as the variability of surface protrusion lengths and the preference for molecules to reside at or away from the tips of surface projections. We also examined how molecular availability should change with increasing compression of the cell against the substrate. Finally, we convolved the distribution of molecules at the interface with a decaying evanescent excitation to predict the fluorescence intensity in total internal reflectance fluorescence microscopy, which can provide a quantitative measure of the relative availability of different molecules at a cell-substrate interface. Model predictions show good agreement with measurements of fluorescence intensity of different molecules labeled fluorescently on the surface of a human neutrophil compressed against a glass surface.

INTRODUCTION

The attachment of leukocytes to a vessel wall during lymphocyte homing or neutrophil recruitment during inflammation involves specific pairs of molecules that must come into close physical contact and react to form a stable bond (1). The ability of a molecule to form a bond depends critically on its position on the cell surface in relation to the cell surface topography. Indeed, molecules such as L-selectin that mediate initial attachment and rolling of cells on the vessel wall tend to be located near the tips of surface folds, whereas other molecules, such as the β_2 integrins, appear to be distributed in the valleys between these folds (2). The relative accessibility of molecules may also be affected by mechanical force between a cell and a substrate. Indeed, we have shown previously that the probability of forming an adhesive bond between β_2 integrins and their binding partner ICAM-1 increases more or less linearly with increasing contact stress (the compressive force per unit area in the contact zone between a cell and the substrate) (3,4). This is consistent with the idea that deformation of the microvilli within the contact zone increases the accessibility of integrins for bond formation. (Note that the term ''microvilli'' is commonly used to describe neutrophil surface topography, although scanning electron micrographs indicate that the surface projections more resemble folds than individual projections. In the following sections, we use the term ''microvilli'' to represent either folds or projections from the cell surface.) Such a mechanism could account for the well-known observation that cell rolling, mediated by selectins, typically precedes firm attachment of cells to a substrate, via integrins (5). During rolling, the combination of fluid shear forces plus adhesive bonds pulling at the rear of the contact zone creates a compressive force between the cell and its substrate in the central and forward regions of contact. This compression should lead to deformation of the microvilli, increased accessibility of integrins to substrate, and increased likelihood that stable integrin bonds will form.

Although all of this makes good sense theoretically, quantitative assessments of the number of accessible bonds in the contact zone between a cell and a substrate have not been reported, to our knowledge. In a companion report in this issue (15), we present a novel methodology using total internal reflectance fluorescence microscopy (TIRFM) to obtain a measure of the relative presence of fluorescently labeled molecules on the cell surface that are in molecularly close contact with the substrate. We used that approach to measure the relative accessibility of four different adhesion molecules on the surface of a living neutrophil resting on a surface, and to determine how this accessibility changes with increasing impingement of the cell onto the substrate. In the following sections, we present a model of the cell surface deformation to gain insights into the physical mechanisms that lead to the behavior we observe. Model predictions are compared to experimental data obtained on two of the four cell adhesion molecules, LFA-1 and L-selectin. A sensitivity analysis is performed to evaluate how sensitive model predictions are when the major parameters are modulated; for instance, when the distribution of the proteins relative to the cell body is changed.

MODEL

The goal of this model is to establish expectations for how the accessibility of molecules (as reflected in their intensity in TIRFM images) should vary depending on the distribution

Submitted December 19, 2008, and accepted for publication April 23, 2009.

*Correspondence: richard_waugh@urmc.rochester.edu

Editor: Levi A. Gheber.

0006-3495/09/07/0369/10 $2.00

doi: 10.1016/j.bpj.2009.04.034

of these molecules relative to the complex microtopography of the cell surface, and depending on the force between the cell and the substrate. First, we use cell mechanics and balance of forces to determine the general shape of the cell contour in the interface. Then we model the cell surface topography in the contact region to account for observations that the height of membrane surface folds is variable. We use a simple linear spring model to gauge how the height of the microvilli will change with increasing force, and generate predictions for the amount of membrane within a certain distance of the substrate as a function of increasing compression. We then assume a distribution (not necessarily uniform) for the position of the molecules relative to the height of a microvillus and obtain a prediction for the density of molecules on the membrane as a function of distance from the surface. Finally, we convolve this with an exponentially decaying evanescent wave to predict the magnitude of intensity in TIRFM images.

Force balance for distributed microvillus lengths

We assume that the cell is in a state of static equilibrium when the TIRFM images are captured and we treat the cell as a viscous liquid drop with a constant uniform cortical tension T_{cort} and a uniform internal pressure. This model was first proposed by Evans and Kukan (6). Although subsequent refinements have been made, particularly in characterizing the dynamics of neutrophil deformation, this basic model of a viscous droplet with a constant cortical tension provides a robust description of the cell in its passive state under static conditions (7,8). The microvilli are approximated as simple springs and we model the cell/glass interface such that it is the force of the microvilli that transmits force from the substrate to the cell surface. Details of this development are supplied in Supporting Material. The shape of the cell surface contour is determined by integration of three simultaneous first-order differential equations,

$$\frac{d\theta}{ds} = \frac{2}{R_c} - \frac{\sin\theta}{r} - \frac{n_v\langle f(\ell_0 + z)\rangle}{T_{\text{cort}}}, \tag{1}$$

$$\frac{dr}{ds} = \cos\theta, \tag{2}$$

$$\frac{dz}{ds} = \sin\theta, \tag{3}$$

where θ and s are the angle of the surface normal with the axis of symmetry and the distance along the surface, respectively (Fig. 1), R_c is the spherical radius of the cell, r is the radial coordinate, n_v is the density of microvilli on the surface, T_{cort} is the cortical tension in the cell, and $\langle f(\ell_0 + z)\rangle$ is the mean force per microvillus. This force is assumed to follow the behavior of a simple spring (9),

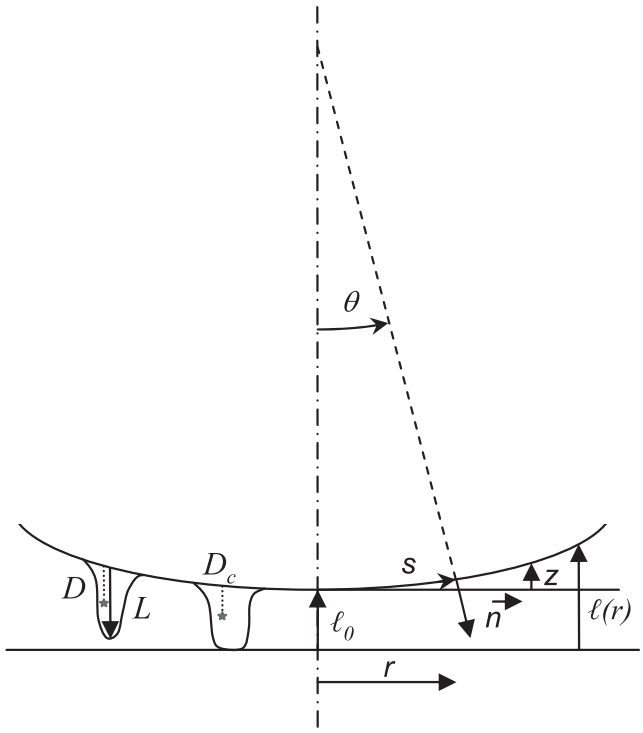

FIGURE 1 Schematic representing a vertical section of the lower part of a neutrophil that is resting above a flat substrate. The value θ is the angle between the cell surface normal $\vec{n}$ and the axis of symmetry passing through the center of the contact zone, r is the radial coordinate measured perpendicular to the axis, s is the arc length or the distance along the (smooth) surface contour, $\ell(r) = \ell_0 + z(r)$, where $\ell(r)$ is the axial separation distance at position r between the spherical contour of the cell and the substrate, ℓ_0 is the separation distance at the center of the contact zone, and $z(r)$ is the axial distance between the surface at the center of the contact zone and the surface location at position r. L represents the length of the microvilli at rest. D and D_c are the distances of the protein relative to the cell body when the microvillus is not compressed and when the microvillus is compressed, respectively.

$$\begin{cases} f = k_v(L - \ell(r)) & \ell < L \\ f = 0 & \ell \geq L \end{cases}, \tag{4}$$

where L is the length of the resting microvillus, and $\ell(r) = \ell_0 + z$ (r) is the distance between the cell body and the substrate. Experimental measurements of microvillus lengths indicate that they are distributed according to a gamma distribution. Thus, the probability density function (pdf) for L is

$$g(L;a,b) = \begin{cases} \dfrac{1}{b^a\Gamma(a)}L^{a-1}e^{-L/b} & \text{if } L > 0 \\ 0 & \text{otherwise} \end{cases}, \tag{5}$$

where $\Gamma(a)$ is the gamma function. Fig. 2 shows the pdfs of gamma distributions we used in this study. Taking into consideration the distribution of microvillus lengths, the average force per microvillus $\langle f\rangle$ becomes

$$\begin{aligned}\langle f\rangle = {} & k_v[ab\{1 - G(\ell(r);a+1,b)\} \\ & - \ell(r)\{1 - G(\ell(r);a,b)\}],\end{aligned} \tag{6}$$

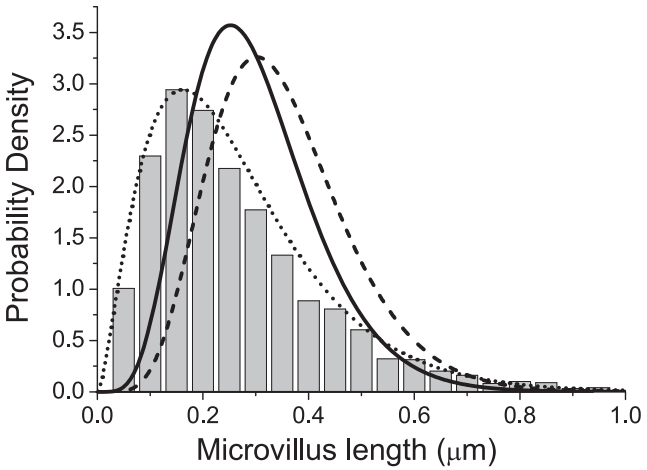

FIGURE 2 Probability density function of the gamma distributions representing the distribution of the microvilli length (in micrometers). Gamma distribution parameters of $a = 2.58$ and $b = 0.103$ correspond to a mean microvilli length of 265 nm and a standard deviation of 165 nm (*dotted line*). This gamma distribution fits the neutrophil microvilli lengths measured by Bruehl et al. (14) and represented by the shaded bars. Also displayed are the gamma distributions that we used in the sensitivity analysis and that fit the measured values reported by Shao et al. (9). Parameters $\{a = 6.25,\ b = 0.048\}$ and $\{a = 7.25, b = 0.048\}$ correspond to the measured values $\{300 \pm 120$ nm (*solid line*)$\}$ and $\{350 \pm 130$ nm (*dashed line*)$\}$, respectively.

where $G(L;a,b) = \int_0^L g(L;a,b)dL$ denotes the cumulative distribution function of the above-defined gamma distribution with parameters a and b. (See Supporting Material for additional details.) The contact stress is the product of the average force per microvillus and the number of microvilli per unit area, $\sigma = n_v \langle f \rangle$. Integrating the contact stress over the whole area of contact of radius R (assuming axis-symmetry) leads to the total force exerted by the microvilli for a given contact area or a given compression of the cell:

$$\text{Total force} = \int_0^R \sigma 2\pi r\, dr. \tag{7}$$

The radius of the contact zone R is taken as the point where the separation distance $\ell(r)$ reaches a value of 615 nm. (See Supporting Material for justification.)

Protein distribution on the cell surface

The relative location of a molecule along the length of a microvillus is conveniently described by a beta distribution. Thus, we express the distance of a protein to the cell body as D (see Fig. 1) such that the ratio $Q = D/L$ is a random variable that follows a beta distribution with parameters c and d:

$$\beta(Q;c,d) = \begin{cases} \dfrac{\Gamma(c+d)}{\Gamma(c)\Gamma(d)} Q^{c-1}(1-Q)^{d-1} & \text{if } Q \in [0,1] \\ 0 & \text{otherwise} \end{cases}. \tag{8}$$

This probability distribution is flexible enough to cover a wide range of situations. For instance, when $c > d$, proteins are more concentrated toward the tip of the microvilli. Conversely, when $c > d$, they segregate toward the cell body between the microvilli. When $c = d = 1$, they are uniformly spread between the tip of the microvilli and the cell body. Example distributions are shown in Results (see also Fig. 5).

When a microvillus is compressed, we assume that the molecular separation distance changes in proportion to the compression of the microvillus. Thus, the molecular distance to the surface on a compressed microvillus D_c is given by

$$D_c = D_c(D,L) = \begin{cases} D & \text{if } L < \ell(r) \\ \ell(r)D/L & \text{otherwise} \end{cases}. \tag{9}$$

TIRF/EPI-intensity ratio

To calculate the intensity of fluorescence in TIRF, we assume that all the proteins are homogeneously fluorescently labeled and that the quantum efficiency ϕ_0 and the molar extinction coefficient ε_0 of the fluorophores are independent of the distance from and the orientation to the glass interface. This assumption is reasonable in light of the fact that the characteristic dimension of surface irregularities (~100 nm) is much larger than the size of the antibodies used to label the surface proteins (~10 nm). The fluorescence intensity measured at the interface and emitted by any fluorophore bound to a protein on a microvillus of initial length L and located at distance D_c from the cell body can be expressed as

$$i^{\text{TIRF}}(\ell(r);D,L) = \phi_0\varepsilon_0 i_0 e^{-[\ell(r)-D_c(\ell(r);D,L)]/d_p}, \tag{10}$$

where i_0 stands for the fluorescence intensity of the fluorophore at distance zero from the interface, and the parameter d_p is the characteristic penetration depth of the evanescent wave,

$$d_p = \frac{\lambda}{4\pi\sqrt{n_1^2 \sin^2\theta_1 - n_2^2}}, \tag{11}$$

where λ is the wavelength of the illumination, n_1 and n_2 are the refractive indices of the cover glass and of the cell, respectively, and θ_1 denotes the angle of incidence of the excitation light (10). Integrating over the distributions for D and L, and accounting for the radial dependence of separation distance beneath the surface contour in the contact zone results in the following expression for the TIRF intensity (see Supporting Material for details):

$$I_{\text{u.a.}}^{\text{TIRF}}(\ell_0) = \frac{2n_0\phi_0\varepsilon_0 i_0}{R^2} \int_0^R \int_0^\infty \int_0^L e^{-[\ell(r)-D_c]/d_p} \times \beta(D/L;c,d)g(L;a,b)r\, dDdLdr. \tag{12}$$

The mean epi-fluorescence intensity per unit area can be expressed as

$$I_{\text{u.a.}}^{\text{EPI}} = n_0\phi_0\varepsilon_0 i_0 \xi, \tag{13}$$

$$R^{\mathrm{Mod}}_{\mathrm{TIRF/EPI}}(\ell_0) = \frac{I^{\mathrm{TIRF}}_{\mathrm{u.a.}}(\ell_0)}{I^{\mathrm{EPI}}_{\mathrm{u.a.}}} = \frac{2}{\xi R^2}\int_0^R\int_0^\infty\int_0^L e^{-[\ell(r)-D_c]/d_p} \times \beta(D/L;c,d)g(L;a,b)r\,dDdLdr, \quad (14)$$

where ξ denotes an unknown constant (identical for all fluorescent molecules, regardless of their distribution relative to surface topography) that both depends on the depth of focus and reflects the difference in amplitude of the incident epi-illumination compared to the TIRF illumination at the interface. Dividing Eq. 12 by Eq. 13, the ratio of $I^{\mathrm{TIRF}}_{\mathrm{u.a.}}(\ell_0)$ versus $I^{\mathrm{EPI}}_{\mathrm{u.a.}}$ for a given compression of the cell can therefore be expressed as
which can be determined up to the constant ξ.

RESULTS

Model constants

In accordance with our experimental setup and observed data (refer to companion report), a few parameters, gathered in Table 1, were kept constant throughout this analysis. We used a diode laser of wavelength $\lambda = 532$ nm, cover glasses of refractive indices $n_1 = 1.516$, and an angle of incidence $\theta_1 = 69°$ for the TIRF illumination. Reichert and Truskey (11) showed that the refractive index of the cell membrane can be neglected, so we used $n_2 = 1.37$, which corresponds to the refractive index of the cell cytoplasm (10). The penetration depth of the evanescent wave d_p was then calculated as 119 nm using Eq. 11. According to our observations on neutrophils, we set n_v, the number of microvilli on the surface, to 1.5 μm^{-2}, and R_c, the radius of the cell, to 4.1 μm. We chose an average value of 20 pN/μm for the cortical tension of the cell T_{cort} (8,12,13).

As an aside, Eqs. 12 and 13 involve n_0, the average number of proteins per unit area of the cell membrane. This parameter was assumed to be constant and independent of the length of the microvilli. This assumption was based on the report by Bruehl et al. (14), who quantified L-selectin distribution on human leukocyte microvilli by immunogold labeling and transmission electron microscopy. The average number of gold particles per microvillus was found to be independent of the microvillus length.

TABLE 1 Optical and cellular constants

Optical constants		
Wavelength of the excitation light	λ	532 nm
Refractive index of the glass	n_1	1.516
Refractive index of the cell cytoplasm	n_2	1.37
TIRF angle of incidence	θ_1	69°
Penetration depth of the evanescent wave	d_p	119 nm
Cell constants		
Cell radius	R_c	4.1 μm
Microvilli density	n_v	1.5 /μm^2
Cortical tension	T_{cort}	20 pN/μm

Microvilli length

Using transmission electron microscopy, Bruehl et al. (14) measured the lengths of human neutrophils' microvilli and provided a histogram of their distribution. This histogram is reproduced in Fig. 2, and it is well represented by a gamma distribution with shape and scale parameters $a = 2.58$ and $b = 0.103$. These parameters correspond to a mean microvilli length of 265 nm and a standard deviation of 165 nm. Using two alternative techniques, scanning electron microscopy and a micropipette manipulation system, Shao et al. (9) estimated the mean and standard deviation of L as 350 ± 130 nm and 300 ± 120 nm, respectively. The parameters of the gamma distributions corresponding to such means and standard deviations were estimated as $a = 7.25$ and $b = 0.048$, and $a = 6.25$ and $b = 0.048$, respectively. Fig. 2 shows the resulting pdfs comparing how the length of the microvilli is distributed under these three sets of parameter estimates. Our primary investigations were based on the parameter estimates obtained from the data of Bruehl et al. (14), because they provided results in better agreement with our own experimental data. Parameter estimates resulting from Shao et al. (9) reported values were considered in a sensitivity analysis, however. The parameters of the gamma distribution, a, b, m_L, and σ_L, both the typical values and the range of values explored in this sensitivity analysis, are summarized in Table 2.

Cell surface contour

The cell surface contour is calculated numerically by integrating simultaneously the three first-order differential equations given by Eqs. 1–3, where $\langle f \rangle$ is replaced by Eq. 6. Besides the parameters $a = 2.58$ and $b = 0.103$ of the gamma distribution of the microvillus lengths, we had to choose a typical value for k_v, the microvillus spring constant. Shao et al. (9) published an estimated value of 43 pN/μm. The values obtained by adjusting the model to the data from our four donors ranged between 28 and 38 pN/μm (see companion article in this issue, (15)). For the calculations here, we use a compromise value of 38 pN/μm, as reported in Table 2. Fig. 3 shows a series of surface contours that were obtained for these typical values by using different starting values for the center spacing ℓ_0: from top to bottom, 500, 300, 200, 150, 125, and 110 nanometers. As the force of compression increases (or ℓ_0 decreases), the curvature of the cell surface gradually decreases before becoming almost flat in an increasing area at the center of the contact zone. For the values of the parameters used here, the value ℓ_0 for which the maximum compression of the microvilli is reached and the cell surface becomes completely flat is 96.86 nm. This suggests that a microvillus of average length 265 nm could be compressed down to almost a third of its initial length.

TABLE 2 Model parameters

	Parameters	Primary values	Alternative values
Gamma distribution (microvilli length)	$m_L \pm \sigma_L$ (nm)	265 ± 165	300 ± 120 and 350 ± 130
	(a, b)	(2.58, 0.103)	(6.25, 0.048) and (7.25, 0.048)
Beta distribution (protein localization)	(c, d)		
	Uniform	(1, 1)	
	Microvilli tips	(3, 1)	(10, 1) and (1, 0.33)
	Cell body	(1, 3)	(1, 10) and (0.33, 1)
Microvillus spring constant	k_v (pN/μm)	38 or 31.9	25, 43, and 75
Vertical distance to the cell body, defines the contact area πR^2	$\ell(R)$ (nm)	615	550 and 680
Experimental constant	ξ	1.6	1.2 and 2.0

Total force

The total force exerted by the microvilli over the whole cell-substrate contact area can be calculated as a function of increasing impingement using Eq. 7 and with the impingement force expressed as a function of contact areas. Fig. 4 displays the resulting curves for three different microvillus spring constant values (from *bottom* to *top*: $k_v = 25$, 43, and 75 pN/μm) using the typical values of microvillus lengths (265 ± 165 nm). The force required to produce a given contact area increases with the spring constant because it takes more force to compress the microvilli to the prespecified separation distance that marks the boundary of the contact zone. In the study described in a companion report (15), contact areas ranged up to 20–25 μm^2, corresponding to predicted forces in the range of 50–100 pN.

Protein distribution on the cell surface

Multiple studies using immunoelectron microscopy have been completed to quantitatively determine the spatial distribution of cell adhesion molecules relative to the cell surface topography (14,16–18). These studies indicate that the cell adhesion molecules under study tend to be systematically positioned preferentially on the microvilli (L-selectin) or on the planar cell body (LFA-1 and Mac-1) of leukocytes. The percentage of molecules in one region or the other ranged from 70 to 90%. The beta distributions that produce the best agreement with our data (refer to companion report (15)) are in very good agreement with these observations. For example, if the parameter d is taken to be 1.0, the values for the parameter c for L-selectin ranged from 2.2 to 3.3, corresponding to 78–90% of the molecules being located in the top half of the microvillus. Values for the parameter d ($c = 1$) that matched data for the integrins LFA-1 and Mac 1 appeared to vary more, from 1.5 to 15.5, corresponding to 60–99% or greater of the molecules in the bottom half of the microvilli. The pdfs for several different molecular distributions are shown in Fig. 5, *A* and *B*.

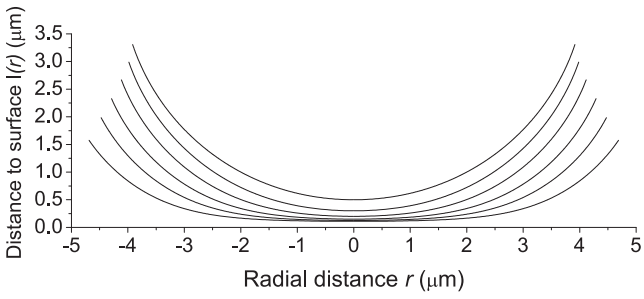

FIGURE 3 Cell surface contour given by the radial coordinate r and the vertical distance from the cell body to the substrate $\ell(r) = \ell_0 + z(r)$ for several impingement forces illustrated by their corresponding distances ℓ_0. From top to bottom, ℓ_0 is equal to 500, 300, 200, 150, 125, and 110 nm. These curves were generated using a microvillus spring constant of 38 pN/μm, and correspond to compressive loads of 1.4, 11.6, 33.8, 68.5, 113.9, and 183.5 pN for the ℓ_0 parameter values used in the calculations.

Effects of protein localization on the TIRF/EPI-intensity ratio

A critical test of the usefulness of the model is to predict behavior observed experimentally. In Fig. 5 *C* are shown data for two different molecules, one that tends to be distributed at the tips of microvilli (L-selectin) and one that tends to

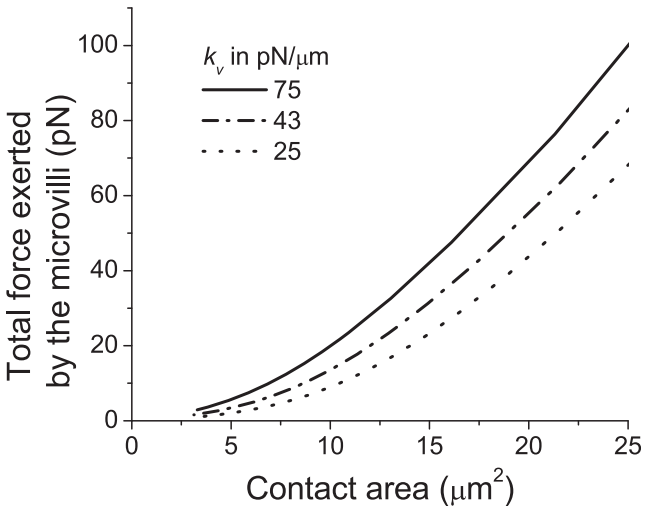

FIGURE 4 Total force exerted by the microvilli calculated over the contact area as a function of increasing impingement for three different microvillus spring constant values (from *bottom* to *top*: $k_v = 25$, 43, and 75 pN/μm). To calculate the contact areas, we used a value of 615 nm for $\ell(R)$, the vertical distance between the cell body and the substrate at the edge radii R of the contact areas.

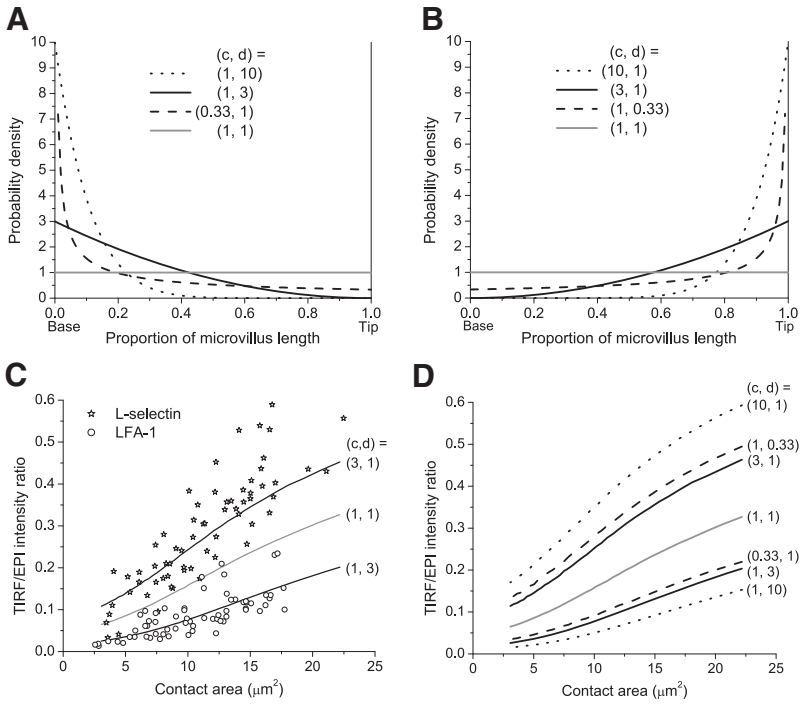

FIGURE 5 (*A* and *B*) Probability density function of the beta distribution illustrating the localization of the proteins along the microvilli. (*A*) When the parameters of the beta-distribution c and d are such that $c < d$, the proteins are predominantly localized on the planar cell body. (*B*) When $c > d$, they are concentrated around the tips of the microvilli. For comparison, the distribution corresponding to $c = d = 1$ is also displayed. In that case, proteins are uniformly distributed along the microvillus length. (*C*) TIRF/EPI-intensity ratio as a function of the contact area. The symbols represent measurements obtained from one donor. Stars represent data for L-selectin and circles represent data for LFA-1. The two solid lines correspond to the model curves adjusted to these experimental data. The corresponding values for the distribution parameters c and d are given in parentheses. For comparison, the model prediction for the uniform protein distribution (*shaded line*) is displayed. (*D*) TIRF/EPI-intensity ratios predicted by the model for the beta distributions displayed in panels *A* and *B*.

be distributed on the cell body (LFA-1). Each point represents a measurement obtained from one TIRF image for one cell under a certain force of impingement. There were seven-to-nine cells tested per protein (refer to companion report (15)). Fig. 5 *C* also shows the $R^{\mathrm{Mod}}_{\mathrm{TIRF/EPI}}$ calculated from Eq. 14 as a function of πR^2 for three characteristic protein distributions: one for molecules distributed preferentially at the microvilli tips (3,1); one with preferential distribution to the cell body (1,3); and one with a uniform distribution (1,1). Other model parameters took on typical values, except for k_v, for which a value equal to 31.9 pN/μm was found to provide a good match between prediction and measurement. The model agrees well with experimental observation that the more the distribution of proteins tends toward the tips of the microvilli, the higher the ratios of fluorescence intensities (TIRF over EPI) and the faster they increase with the contact area. As expected, ratios obtained for the case where proteins are uniformly spread on the cell surface are intermediate between ratios obtained for proteins located on the tips of the microvilli and proteins concentrated on the cell body. Overall, as shown in Fig. 5 *C*, the $R^{\mathrm{Mod}}_{\mathrm{TIRF/EPI}}$ varies substantially by changing the values of either c or d. Thus, as expected, proteins that are dissimilarly localized on the microvilli result in dissimilar ratios of TIRF/EPI-intensity.

The values for c and d in the beta distribution can be varied over a wide range, and different pairs of values may produce similar distributions. Nevertheless, a few general trends as to how changing the molecular distribution is predicted to affect the TIRF/EPI ratio, are evident. When $c > d$, the proteins will segregate more toward the tips of the microvilli. As a consequence, the ratio $R^{\mathrm{Mod}}_{\mathrm{TIRF/EPI}}$ will

1. Have a higher initial value.
2. Increase faster with the surface of contact.
3. Reach higher values for the largest contact area.

This is illustrated in Fig. 5 *D* when c increases from 3 to 10, with the value of d remaining equal to one. When $d > c$, the proteins will segregate more toward the cell body, and the ratio $R^{\mathrm{Mod}}_{\mathrm{TIRF/EPI}}$ will

1. Have a lower initial value.
2. Increase more slowly as a function of the contact area.
3. Reach smaller values for the largest contact areas.

Again, this is illustrated in Fig. 5 *D* when d is increased from 3 to 10, with c equal to one. In summary, the ratios TIRF over EPI will drift farther apart from the uniform distribution as the proteins concentrate more toward the extremities of the microvilli (that is, either their tip or the cell body).

All pairs of values (c, d) satisfying $c > d$ would describe a situation where proteins tend to segregate closer to the tip of the microvilli than to the body of the cell. By selecting appropriate values for these parameters, one can modulate not only how close to the tip of the microvilli the proteins are located, but also the shape of the distribution. For instance, beta distributions with parameters (3, 1) and (1, 0.33) would both distribute 70% of the proteins on the upper third of the microvillus length (see Fig. 5 *B*). However, the proteins would be distributed quite differently over the length of the microvilli under these two scenarios. Although the resultant values for the TIRF/EPI ratio predicted by our model are different in these two cases (see Fig. 5 *D*), these predictions do not differ substantially. Conversely, whenever $d > c$, proteins tend to be distributed toward the cell body, and different values of these

constants can produce different protein distributions but they would still provide similar predictions for the TIRF/EPI ratio (Fig. 5, *A* and *D*). To limit the range of possibilities when comparing model predictions to the data, we have arbitrarily chosen the smaller of the two parameters (c and d) to be 1.0. To adjust the model predictions to the observations, we varied the value of the other parameter.

SENSITIVITY ANALYSIS

Gamma distribution for the microvilli lengths

Although we have done our best to match the distribution of microvilli lengths to published measurements, we recognize the potential for measurement error in determining these distributions. Indeed, different studies have produced different means and variances for the distribution of microvilli lengths. Therefore, understanding how changes in the distribution might affect model predictions is of interest. This is illustrated in Fig. 6 *A*, where the three gamma distributions shown in Fig. 2 are used to generate different model predictions. All $R^{\mathrm{Mod}}_{\mathrm{TIRF/EPI}}$ were calculated using the primary parameters listed in Table 2 ($k_v = 38$ pN/μm). Interestingly, the model predictions remain similar when using any of the three gamma distributions resulting from literature reports. Although the effect of changing the distribution of the length is more pronounced for molecules concentrated around the tip of the microvilli than for those sequestered near the cell body, in all cases, the changes are not as dramatic as when altering the distribution of proteins along the microvilli. The importance of having a distribution of microvilli lengths is demonstrated by considering the case where all microvilli are assumed to have the same length of 300 nm. As observed in Fig. 6 *A*, when microvilli have a constant length instead of variable lengths, the predictions of the ratio $R^{\mathrm{Mod}}_{\mathrm{TIRF/EPI}}$ as a function of area exhibit a distinct, steplike behavior that is less consistent with experimental observations. The ratio $R^{\mathrm{Mod}}_{\mathrm{TIRF/EPI}}$ becomes a smoother function of the contact area when the variance of the length of the microvilli increases.

Microvillus spring constant

The choice of the microvillus spring constant k_v can have significant effects on the predicted dependence of the TIRF/EPI ratio as a function of contact area (See Fig. 6 *B*). The range of possible values for k_v has a lower bound that is determined by the cortical tension of the cell and the density of microvilli on the surface. According to Eq. S4 (found in Supporting Material), the smallest feasible value of the microvillus spring constant k_v is 24.54 pN/μm for the primary parameters reported in Table 2. The effect of k_v on the ratios $R^{\mathrm{Mod}}_{\mathrm{TIRF/EPI}}$ as a function of the contact area for three values in the allowable range are shown in Fig. 6 *B* (from *top* to *bottom*, $k_v = 25$, 43, and 75 pN/μm). The remaining model parameters were set to the typical values given in Table 2. As one can see in Fig. 6 *B*, changing k_v primarily alters the slope of the model predictions. For each protein distribution (microvilli tips or cell body), the three ratios $R^{\mathrm{Mod}}_{\mathrm{TIRF/EPI}}$ start around the same value before drifting apart with increasing contact area. The smaller the k_v, the faster the ratio increases with increasing contact area. The sensitivity of the model predictions to k_v makes this an important parameter when searching for agreement between model predictions and experimental observations.

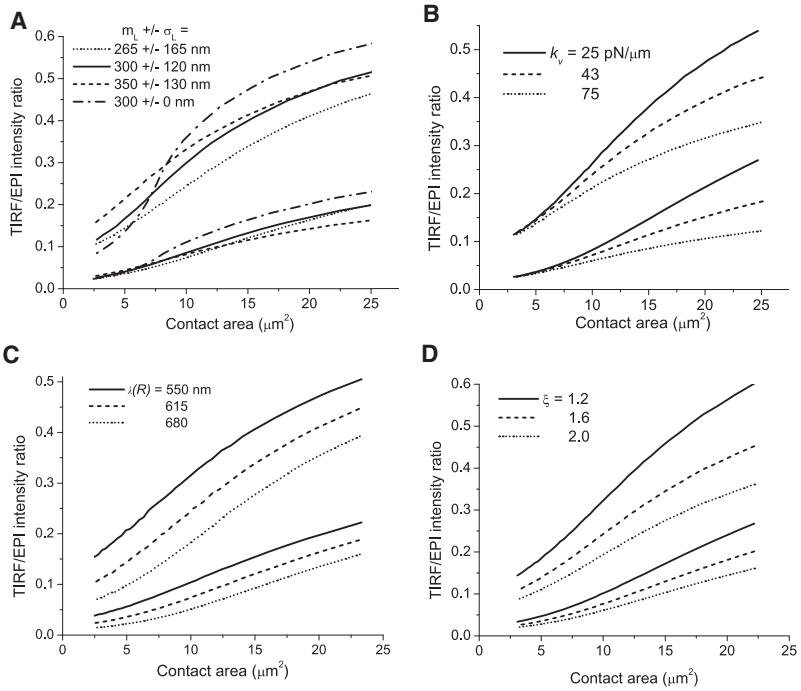

FIGURE 6 Effect of (*A*) the gamma distribution of the microvillus length; (*B*) the microvillus spring constant k_v; (*C*) the vertical distance $\ell(R)$ from the substrate to the cell body at radial position R; and (*D*) the coefficient ξ on the TIRF/EPI-intensity ratio predictions as a function of the contact area. All four panels show model predictions for the two typical beta distributions with parameters (c, d) = (3,1) and (1,3). When not specified, model parameters are given primary values. Three of the four gamma-distributions studied in panel *A* are represented in Fig. 2. The dotted, solid, and dashed curves stand for the microvilli length distributions 265 ± 165 nm, 300 ± 120 nm, and 350 ± 130 nm, respectively. The dotted-dashed curve corresponds to the case when the microvillus length is given a single value of 300 nm.

Vertical distance ℓ at radial position R

The contact area πR^2 over which $R^{\mathrm{Mod}}_{\mathrm{TIRF/EPI}}$ is calculated, depends on the vertical distance ℓ from the glass surface to the cell body at radial position R. We selected a value of 615 nm based on observations made on resting neutrophils. To explore the influence of the value chosen for $\ell(R)$ on the ratios, we calculated them for two other values of $\ell(R)$, specifically 550 and 680 nm. Fig. 6 *C* shows that the ratio $R^{\mathrm{Mod}}_{\mathrm{TIRF/EPI}}$ decreases with increasing $\ell(R)$. For a given distribution of the protein, the value of the decrease in $R^{\mathrm{Mod}}_{\mathrm{TIRF/EPI}}$ is very similar for all contact areas. Thus, the main effect of varying $\ell(R)$ is to change the effective intercept of the model predictions. The reason for this decrease lies in the way $R^{\mathrm{Mod}}_{\mathrm{TIRF/EPI}}$ is calculated. Even though $R^{\mathrm{Mod}}_{\mathrm{TIRF/EPI}}$ corresponds to the ratio of the intensities per unit area, it is calculated by integrating the TIRF intensity over the whole contact area, divided by the surface area. Therefore, the higher the $\ell(R)$, the higher the radius R, and the bigger the contact area. In such circumstances, the TIRF intensity per unit area is reduced. Experimentally, we have endeavored to be consistent in the way in which we choose the contact area for measurement. Therefore, the value of $\ell(R)$ is held constant for all donors and all different types of molecules.

Experimental constant ξ

The coefficient ξ is a physical parameter that depends on the depth of focus, and reflects the difference in intensity of the incident epi-illumination compared to the TIRF illumination at the interface. This coefficient could be affected by several factors, especially the experimental setup (microscope, objective, illuminations, etc.). From a practical standpoint, ξ cannot be smaller than one. We found that coefficients ξ ranging from 1.24 to 2.33 provided the best agreement between model predictions and experimental results. Fig. 6 *D* illustrates how changing ξ affects the ratios. Increasing ξ lowers the $R^{\mathrm{Mod}}_{\mathrm{TIRF/EPI}}$ values for all values of the contact area. In addition, for a given distribution of the protein, the decrease in the value of $R^{\mathrm{Mod}}_{\mathrm{TIRF/EPI}}$ becomes more and more significant with increasing contact area. Thus, ξ acts as a scaling factor that depends principally on the physical setup of the microscope.

DISCUSSION

The accessibility of adhesion molecules to their binding partners is a critical factor in bond formation during leukocyte adhesion. The distribution of molecules relative to the cell surface topography can have a substantial effect on the kinetics of bond formation between cells and substrates. The model described here provides a framework for the quantitative assessment of molecular availability that accounts for a number of important physical features of the cell surface and the distribution of molecules on the surface. Specifically, we have accounted for the deformability of the cell surface and the balance of forces in the interface, as well as the variability of surface protrusion lengths and the preference for molecules to reside at or away from the tips of surface projections. We have also convolved the distribution of molecules at the interface with a decaying evanescent excitation illumination to predict the fluorescence intensity in TIRF microscopy, and shown good fidelity between the model predictions and experimental observations. Although the model is complex, and includes a number of parameters that can be adjusted to obtain agreement between theory and experiment, simpler modeling approaches provided a poor match to experimental observation. Bruehl et al. (14) and Shao et al. (9) have established that microvilli have dissimilar lengths, and that their length can vary dramatically, even among microvilli of the same cell. Failure to account for this characteristic of the cell surface results in a too-abrupt change in fluorescence intensity as the cell is compressed onto a surface. An even simpler model in which the contact zone was regarded as a uniform layer with a molecular concentration that varied with distance from the cell surface resulted in an even poorer match to the data (not shown). In this case, although molecules located near the tips, far from the cell surface, gave higher intensities than molecules located near the cell surface, there was little change in signal as the layer was compressed, and there was no apparent difference in how much the intensity increased with compression for the different molecular distributions. This was in sharp disagreement with experimental observation. Thus, both the distribution of microvillus lengths and an accurate accounting of the mechanics of the cell-substrate interaction, including changes in surface contour and compression of the microvilli in the interface, are critical elements of the model.

An early finding in the investigation of leukocyte adhesion to endothelial ligands in shear flow was that firm attachment of cells via integrin bonding was greatly facilitated by prior rolling interactions mediated by selectins (19). Our interest in the change in the concentration of molecules at the interface with compression was motivated by the question: How much was this enhancement simply due to an increase in the accessibility of integrins to the substrate from the compression of the cell onto the substrate during rolling? The forces of interaction produced during cell rolling are comparable to those estimated from our model analysis. Based on the work of Goldman et al. (20), and as previously discussed in Spillmann et al. (21), a shear force of 2.0 dyn/cm^2 (0.2 N/m^2) should produce a torque on a spherical cell of radius 4.0 μm of ~4×10^{-16} Nm. This would be balanced by a reaction force of ~125 pN and a contact area ≈ 35 μm^2. If the enhancement of integrin binding as a result of cell rolling were simply due to a mechanical effect, we expected to see a substantial increase in the presence of integrins at the interface at this level of force. Consistent with this expectation, there is an increase of five- to 10-fold in the presence of integrins at the interface at this level of force and contact area compared to cells resting lightly on the surface. Interestingly, the increase in surface accessibility for molecules located at the tips of microvilli also increased substantially, similar on a fractional basis, but

much larger in absolute terms. This indicates that rolling interactions should be self-reinforcing, in that once rolling starts, substantially more molecules become available at the interface for further bond formation. Consideration of the model features that lead to this prediction indicates that the primary mechanism for increasing molecular presence at the interface with compression is that more and more microvilli are brought into contact with the surface, rather than the alternative aspect that the cell surface is drawing closer to the substrate. The increase in microvillus contact is not simply the result of increasing the macroscopic contact area, as the predictions are already normalized for contact area. Rather, as the longest microvilli are compressed, shorter microvilli, previously not reaching the surface, begin to come into contact.

The fact that the number of molecules per unit area at the interface increases so substantially with increasing contact area may at first seem to contradict a prior report from our laboratory that the probability of adhesion increases linearly with contact area. (See Figs. 3 and 4 in (21).) Bimolecular reaction theory indicates that the formation of a bond at the interface should depend on the product of the density of adhesion molecules at the interface and the contact area. Thus, if both the number per unit area and the area are increasing, as our current study indicates, the dependence of bond formation on contact area should increase more than linearly. In considering this apparent contradiction, we note that the contact stress σ in the two experiments was markedly different because of the curvature of the substrate. A model of the cell as a fluid droplet leads to (21)

$$\sigma = T_{\text{cort}}\left(\frac{1}{R_c} + \frac{1}{R_s}\right), \tag{15}$$

where R_s is the radius of curvature of the substrate. In this study, $1/R_s = 0$, whereas previously, $1/R_s = 0.44$. Thus the contact stress was ~3× as large in the previous study as in this one, which should have caused more complete compression of microvilli in the interface. Note that although the compression of an individual microvillus is assumed to be linear, the compression of the interface is expected to be nonlinear because of the increasing numbers of microvilli engaged at the surface as the longest microvilli are compressed. At higher contact stress, the resistance to compression becomes larger, leading to a slower increase in the concentration of molecules at the interface with further compression. It is worthy of note that some nonlinearity in behavior was observed in our prior study, but only at the lowest contact areas tested. We originally attributed this to measurement error, but it is possible that this was a reflection of the higher than linear dependence of bond formation on area predicted from our current model.

An important distinction between this analysis and cell rolling in vivo is the assumption that the cell has reached a mechanical equilibrium with the substrate. This approach neglects potential contributions to the forces of interaction from the viscous resistance of the cell to rate of deformation. In a previous report, we examined the rate of change of contact area between a cell and a stationary surface under a constant load (7). Theory and measurement both showed that an equilibrium contact area was approached rapidly, such that the contact area was within 10–20% of the equilibrium value within 1.0 s. This rapid rate of relaxation indicates that the assumption of equilibrium is a good one for the experiments described in a companion report, where the cell is stationary on the glass for several seconds before measurement. It would also be reasonable when the rate of cell rolling in vivo is low, such that the portion of the cell membrane in contact with substrate remains so for periods of a few seconds. However, this would require rolling velocities of ~1.0 μm/s, 10–100 times slower than rolling velocities typically measured in vivo (22). The consequence of this is that the contact area in vivo is likely to be smaller than predicted by our analysis, but the contact stress is likely to be larger, as the same forces are distributed over a smaller area. The former effect would tend to reduce the likelihood of bond formation, but the latter would tend to increase (significantly) the number of molecules in the interface available for binding, as the greater contact stress would lead to greater compression of the microvilli in the interface.

CONCLUSIONS

A model of the cell interface during cell compression accounts for observed changes in the relative fluorescence obtained in TIRF microscopy for molecules with different distributions relative to the cell surface topography. Critical elements of the modeling include a nonuniform distribution of microvillus lengths from the cell surface, compressible microvilli, and calculation of the global surface curvature from mechanical force balance. The model is applied in a companion report (15) to examine the surface accessibility of four principal adhesion molecules on neutrophils and changes in their accessibility with compression.

SUPPORTING MATERIAL

Nineteen equations are available at http://www.biophysj.org/biophysj/supplemental/S0006-3495(09)00899-6.

This research was supported by the National Institutes of Health (grant No. PO1-HL18208 to R.E.W. and S.A.H., and grant No. R01-CA134839 to O.H.).

REFERENCES

1. Springer, T. A. 1995. Traffic signals on endothelium for lymphocyte recirculation and leukocyte emigration. *Annu. Rev. Physiol.* 57:827–872.
2. Erlandsen, S. L., S. R. Hasslen, and R. D. Nelson. 1993. Detection and spatial distribution of the β2 integrin (Mac-1) and L-selectin (LECAM-1) adherence receptors on human neutrophils by high-resolution field emission SEM. *J. Histochem. Cytochem.* 41:327–333.
3. Lomakina, E. B., and R. E. Waugh. 2004. Micromechanical tests of adhesion dynamics between neutrophils and immobilized ICAM-1. *Biophys. J.* 86:1223–1233.

4. Lomakina, E. B., and R. E. Waugh. 2006. Bond formation during cell compression. *In* Cellular Engineering. M. R. King, editor. Elsevier, Burlington, MA.
5. Lawrence, M. B., and T. A. Springer. 1991. Leukocytes roll on a selectin at physiologic flow rates: distinction from and prerequisite for adhesion through integrins. *Cell*. 65:859–873.
6. Evans, E., and B. Kukan. 1984. Passive material behavior of granulocytes based on large deformation and recovery after deformation tests. *Blood*. 64:1028–1035.
7. Lomakina, E. B., C. M. Spillmann, M. R. King, and R. E. Waugh. 2004. Rheological analysis and measurement of neutrophil indentation. *Biophys. J*. 87:4246–4258.
8. Needham, D., and R. M. Hochmuth. 1992. A sensitive measure of surface stress in the resting neutrophil. *Biophys. J*. 61:1664–1670.
9. Shao, J. Y., H. P. Ting-Beall, and R. M. Hochmuth. 1998. Static and dynamic lengths of neutrophil microvilli. *Proc. Natl. Acad. Sci. USA*. 95:6797–6802.
10. Gingell, D., O. S. Heavens, and J. S. Mellor. 1987. General electromagnetic theory of total internal reflection fluorescence: the quantitative basis for mapping cell-substratum topography. *J. Cell Sci*. 87:677–693.
11. Reichert, W. M., and G. A. Truskey. 1990. Total internal reflection fluorescence (TIRF) microscopy. I. Modeling cell contact region fluorescence. *J. Cell Sci*. 96:219–230.
12. Evans, E., and A. Yeung. 1989. Apparent viscosity and cortical tension of blood granulocytes determined by micropipette aspiration. *Biophys. J*. 56:151–160.
13. Tsai, M. A., R. S. Frank, and R. E. Waugh. 1994. Passive mechanical behavior of human neutrophils: effect of cytochalasin B. *Biophys. J*. 66:2166–2172.
14. Bruehl, R. E., T. A. Springer, and D. F. Bainton. 1996. Quantitation of L-selectin distribution on human leukocyte microvilli by immunogold labeling and electron microscopy. *J. Histochem. Cytochem*. 44:835–844.
15. Hocdé, S. A., O. Hyrien, and R. E. Waugh. 2009. Cell adhesion molecule distribution relative to neutrophil surface topography assessed by TIRFM. *Biophys. J*. 97:379–387.
16. Berlin, C., R. F. Bargatze, J. J. Campbell, U. H. von Andrian, M. C. Szabo, et al. 1995. α4 integrins mediate lymphocyte attachment and rolling under physiologic flow. *Cell*. 80:413–422.
17. Abitorabi, M. A., R. K. Pachynski, R. E. Ferrando, M. Tidswell, and D. J. Erle. 1997. Presentation of integrins on leukocyte microvilli: a role for the extracellular domain in determining membrane localization. *J. Cell Biol*. 139:563–571.
18. von Andrian, U. H., S. R. Hasslen, R. D. Nelson, S. L. Erlandsen, and E. C. Butcher. 1995. A central role for microvillus receptor presentation in leukocyte adhesion under flow. *Cell*. 82:989–999.
19. Lawrence, M. B., E. L. Berg, E. C. Butcher, and T. A. Springer. 1995. Rolling of lymphocytes and neutrophils on peripheral node addressin and subsequent arrest on ICAM-1 in shear flow. *Eur. J. Immunol*. 25:1025–1031.
20. Goldman, A. J., R. G. Cox, and H. Brenner. 1967. Slow viscous motion of a sphere parallel to a plane wall: II. Couette flow. *Chem. Eng. Sci*. 22:653–660.
21. Spillmann, C. M., E. Lomakina, and R. E. Waugh. 2004. Neutrophil adhesive contact dependence on impingement force. *Biophys. J*. 87:4237–4245.
22. Kim, M. B., and I. H. Sarelius. 2004. Role of shear forces and adhesion molecule distribution on P-selectin-mediated leukocyte rolling in postcapillary venules. *Am. J. Physiol. Heart Circ. Physiol*. 287:H2705–H2711.